[PS]Chemostratigraphy of the Woodbine and Eagle Ford Groups, Brazos Basin, Texas*

Melissa Meyer[1,2], Michael Pope[1], and Arthur Donovan[1]

Search and Discovery Article #11237 (2019)**
Posted July 29, 2019

*Adapted from poster presentation given at 2019 AAPG Annual Convention and Exhibition, San Antonio, Texas, May 19-22, 2019
 DOI:10.1306/11237Meyer2019

[1]Texas A&M University, College Station, Texas (mjmeyer87@gmail.com)
[2]Apace Corporation, Houston, Texas

Abstract

In the Cenomanian-Turonian Woodbine and Eagle Ford Groups in the Brazos Basin, XRF chemostratigraphy highlights significant mudstone chemical heterogeneities that are often difficult to observe or quantify at the macroscale. Several key elements, Ca, Si, Mo, Mn, and Ni, were correlated to depositional conditions and used in a hierarchical cluster analysis to characterize five chemofacies across ten cores in the Woodbine and Eagle Ford groups: (1) argillaceous, OM-poor; (2) transitional, OM-poor; (3) transitional, OM-moderate; (4) calcareous, OM-rich; and (5) calcareous, OM-moderate. Characterizations of organic matter richness, mineralogy, and environmental conditions of deposition were established by correlations between key element abundances, TOC measurements, XRD measurements, and petrographic observations of lithologic composition, bioturbation, and sedimentary textures. Combined observation redox-sensitive trace element enrichment and petrographically observed textures indicate that all chemofacies were deposited in an intra-shelf basin above storm-wave base. The most organic-rich chemofacies was deposited on a dysoxic (not anoxic) distal shelf. Mudstone organic matter enrichment is driven dominantly by the minimization of siliciclastic dilution and secondarily enhanced by oxygen-restriction.

Regional correlations of chemofacies within a sequence stratigraphic framework developed from previous outcrop and subsurface work indicates a clear relationship between interpreted stratigraphy and chemofacies deposition. Generally, the highstand sequence sets of the Woodbine Group and Upper Eagle Ford Formation are dominated by clay-rich, OM-lean, siliciclastic dilution and contain poor quality source rock. Conversely, the transgressive sequence set of the Lower Eagle Ford Formation is dominated by OM-rich pelagic carbonate accumulation and contains excellent quality source rock.

Depositional Environment and Source Rock Quality Characterization of the Woodbine and Eagle Ford Groups, Brazos Basin, Texas: An Integrated Chemostratigraphic, Sequence Stratigraphic, and Petrographic Approach

Melissa J. Meyer[1,2], Arthur D. Donovan[1], Michael C. Pope[1]

1. Department of Geology and Geophysics, Texas A&M University, College Station, Texas, United States
2. Apache Corporation, 2000 Post Oak Boulevard #100, Houston, Texas, United States

Apache

A&M GEOSCIENCES

KEY ELEMENTAL PROXIES

Ca - Enrichment = Carbonate Input

Si+Al+Ti+K Enrichment = Clay-Rich Siliciclastic Input

Mo Enrichment = Oxygen Restricted Deposition

Mn Enrichment = Oxygen-Rich Deposition

Ni Enrichment = Organic Matter Paleoproductivity

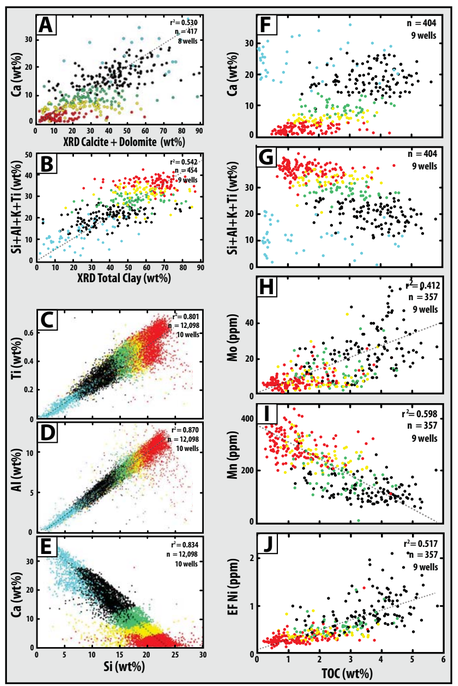

Figure 7. Cross-plots of elemental, mineral data, and TOC data, colored by chemofacies.

CHEMOFACIES CHARACTERIZATION

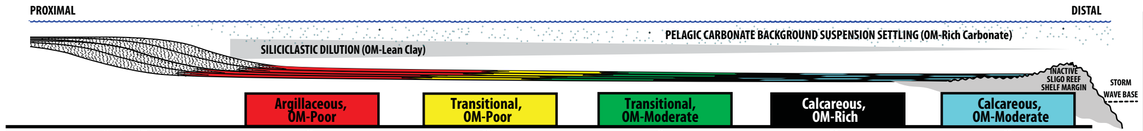

		Argillaceous, OM-Poor	Transitional, OM-Poor	Transitional, OM-Moderate	Calcareous, OM-Rich	Calcareous, OM-Moderate
Petrographic Characteristics	Number of Thin Sections	61	29	61	56	22
	Dominant Lithology	Parallel-Laminated, Argillaceous, Medium to Fine Mudstone	Wavy-Parallel, Argillaceous, Fine Mudstone	Wavy-Discontinuous, Foraminiferal Argillaceous-Calcareous, Fine Mudstone	Wavy-Discontinuous, Foraminiferal, Calcareous, Fine Mudstone	Dolomitized, Foraminiferal Calcareous Fine Mudstone and Fibrous Calcite Cement
	Visual Mineralogical Estimation	> 90% clay-rich siliciclastics < 10% calcareous material (planktonic fecal pellets and foraminifera)	70 - 90% clay-rich siliciclastics 10 - 30% calcareous material (planktonic fecal pellets and foraminifera)	50 - 70% clay-rich siliciclastics 30 - 50% calcareous material (planktonic fecal pellets and foraminifera)	20 - 50% clay-rich siliciclastics 50 - 80% calcareous material (planktonic fecal pellets and foraminifera)	< 20% clay-rich siliciclastics 80 - 100% carbonate diagenetic cement, planktonic fecal pellets, and foraminifera)
	Bioturbation Index (Table 3)	0 - 5	1 - 5	2 - 4	1 - 2	0 - 1
	Sediment Energy Index (Table 4)	3 - 4	3 - 4	2 - 3	1 - 2	1 - 4
Depositional Environment		Oxygenated, Pro-Delta (Proximal) Shelf Above Storm Wave Base	Oxygenated Pro-Delta (Medial) Shelf Above Storm Wave Base	Oxygenated to Dysoxic Pro-Delta (Distal) Shelf Above Storm Wave Base	Dysoxic Open Marine Shelf Above Storm Wave Base	Early Diagenetic
XRF Elemental Averages	Total Number of Measurements	4,061 (33%)	1,964 (16%)	2,118 (17%)	3,030 (24%)	550 (5%)
	Total Represented Footage of Core	812' (247 m)	393' (120 m)	423' (129 m)	606' (212 m)	110' (36 m)
	Carbonate Index: Ca	2 wt%	6 wt%	9 wt%	17 wt%	25 wt%
	Terrigenous Index: Si + Al + K + Ti	37 wt%	32 wt%	29 wt%	21 wt%	10 wt%
	Oxygen Indicator: Mn	325 ppm	241 ppm	175 ppm	116 ppm	162 ppm**
	Anoxia Indicator: EF Mo	10	16	20	33	7**
	Paleoproductivity Indicator: EF Ni	0.45	0.71	0.73	1.2	0.27**
XRD Mineralogy Averages	Total XRD Measurements	173	99	96	181	42
	Total Carbonate	24 wt%	26 wt%	30 wt%	40 wt%	50 wt%
	Total Clay	46 wt%	47 wt%	44 wt%	36 wt%	27 wt%
	Quartz and Feldspar	17 wt%	15 wt%	12 wt%	15 wt%	15 wt%
TOC Averages	Total TOC Measurements	160	78	72	161	32
	Average TOC	1.47 wt%	2.42 wt%	2.81 wt%	3.70 wt%	2.85 wt%
Rebound Hammer Strength Averages	Total Number of Measurements	514	194	185	360	58
	Uniaxial Compressive Strength	2,915 psi	3,088 psi	3,443 psi	4,512 psi	6,368 psi

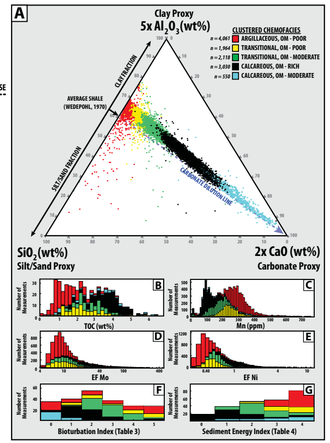

Figure 8. (Left) Summary parameters for each chemofacies and a depositional model for the spectrum of facies observed.

Figure 9. (Above) Elemental ternary and histogram distributions of key parameters, colored by chemofacies.

Figure 15. (Below) Hand-contoured denisty cross-plots for bioturbation index (Table 2) and interpretted sediment energy index (Table 3), measured from 233 thin section characterizations. Sediment energy index is interpretted from observed sedimentary textures. Cross-plots indicate that, in general, bioturbation increases with increasing sediment reworking. The most oxygen-restricted facies, the calcareous, OM-rich chemofacies, shows significant degrees of bioturbation and sediment reworking and thus is interpretted to be, at most, dysonic. The calcareous, OM-moderate chemofacies is diagenetic, showing no bioturbation.

PETROGRAPHY

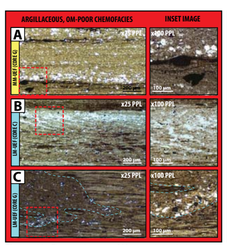

Figure 10. The argillaceous, OM-poor chemofacies occurs primarily as a parallel laminated argillaceous medium to fine mudstone.

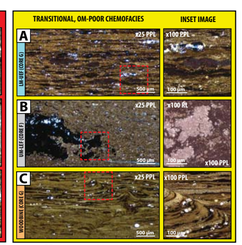

Figure 11. The transitional, OM-poor chemofacies occurs primarily as a wavy-parallel to wavy-discontinuous, laminated argillaceous fine mudstone.

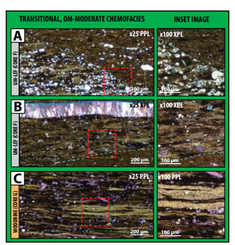

Figure 12. The transitional, OM-moderate chemofacies occurs primarily as a wavy-discontinuous, foraminiferal argillaceous-calcareous fine mudstone.

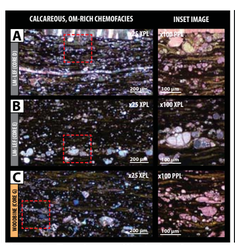

Figure 13. The calcareous, OM-rich chemofacies occurs primarily as a wavy-discontinuous, foraminiferal calcareous fine mudstone.

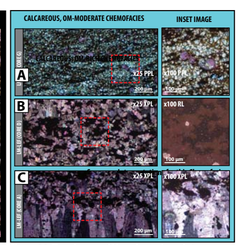

Figure 14. The calcareous, OM-moderate chemofacies occurs as two distinct diagenetic carbonates: a dolomitized foraminiferal calcareous fine mudstone (Figure 14A) and a thinly-bedded fibrous, calcite cement (Figure 14B and C).

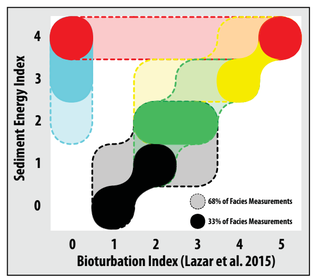

STRATIGRAPHIC CHARACTERIZATION

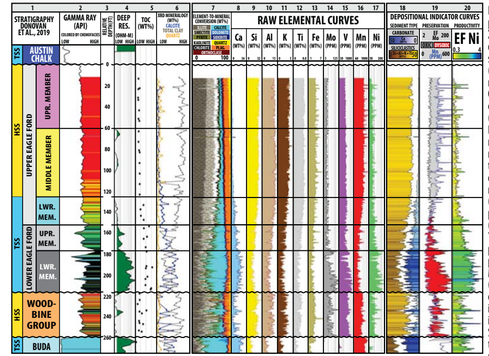

Figure 16. (Left) Geochemical profiles for Core D as correlated to TOC, XRD mineralogy, gamma-ray logs and deep-resistivity logs. Well location is shown in Figure 1. Track descriptions: (1) Sequence stratigraphic nomenclature used for this study. (2) Gamma-ray profile colored by chemofacies where core is available. (3) Relative depth track. (4) Deep-resistivity profile. (5) TOC measurements from core. (6) XRD mineralogy measurements of calcite, total clay, and quartz. (7) An element-to-mineral conversion model, calibrated to XRD mineralogy. (8) Calcium (Ca) profile. (9) Silicon (Si) profile. (10) Aluminum (Al) profile. (11) Potassium (K) profile. (12) Titanium (Ti) profile. (13) Iron (Fe) profile. (14) Molybdenum (Mo) profile. (15) Vandium (V) profile. (16) Manganese (Mn) profile. (17) Nickel (Ni) profile. (18) Sediment type characterized by both carbonate input and clastic dilution. Carbonate input is represented by calcium (Ca). Siliciclastic dilution is represented by the sum of silicon (Si), aluminum (Al), potassium (K), and titanium (Ti). Note the reciprocal nature of the two sediment types. (19) Organic matter (OM) preservation index indicated by the crossover of molybdenum (Mo) and manganese (Mn), which indicate reciprocal conditions of water column oxygenation (Mo enrichment = dysoxic, Mn enrichment = oxygenated). (20) Paleoproductivity indicator represented by enrichment factor nickel (EF Ni).

Table 4. Summary of the defining characteristics of each stratigraphic unit.

Stratigraphic Unit	Dominant Chemofacies	Clay-Dominated Siliciclastic Dilution	Redox Conditions	Organic Matter Productivity	Source Rock Quality
MM-UEF	Argillaceous, OM - Poor	High	Oxygenated	Low	Poor
LM-UEF	Transitional, OM - Poor	High	Oxygenated	Low	Poor
UM-LEF	Transitional OM - Moderate	Moderate	Suboxic	Moderate	Fair to Good
LM-LEF	Calcareous, OM - Rich	Low	Dysoxic	High	Good
WOODBINE	Argillaceous, OM - Poor	High	Suboxic	Moderate	Fair

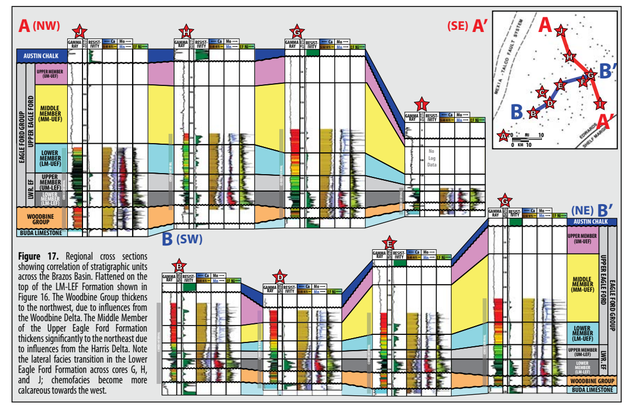

Figure 17. Regional cross sections showing correlation of stratigraphic units across the Brazos Basin. Flattened on the top of the LM-LEF Formation shown in Figure 16. The Woodbine Group thickens to the northwest, due to influences from the Woodbine Delta. The Middle Member of the Upper Eagle Ford Formation thickens significantly to the northeast due to influences from the Harris Delta. Note the lateral facies transition in the Lower Eagle Ford Formation across cores G, H, and J; chemofacies become more calcareous towards the west.

BACKGROUND INFORMATION

ABSTRACT

The XRF chemostratigraphy of the Cenomanian-Turonian Woodbine and Eagle Ford Groups in the Brazos Basin was used to identify distinct chemofacies within a regionally correlative sequence stratigraphic framework. Chemostratigraphic correlations of high-resolution XRF measurements collected from ten cored wells highlight significant vertical and lateral chemical heterogeneities in these mudstones. Several key elements —Ca, Si, Mo, Mn, and Ni— were correlated to depositional conditions and used in a hierarchical cluster analysis to characterize five chemofacies throughout the Woodbine and Eagle Ford Groups: (1) argillaceous, OM-poor; (2) transitional, OM-poor; (3) transitional, OM-moderate; (4) calcareous, OM-rich; and (5) calcareous, OM-moderate. Characterizations of OM-richness, mineralogy, and environmental conditions of deposition were established by correlations between key element abundances, TOC measurements, XRD measurements, and petrographic observations of lithologic composition, bioturbation, and sedimentary textures. Although significantly enriched in redox-sensitive indicators, petrographic observations indicate that the most organic-rich facies was deposited within storm-wave base in a dysoxic environment with intermittent bottom-water current energy and bioturbation. Organic matter enrichment is achieved primarily through the minimization of siliciclastic dilution, not anoxia.

Five temporally and chemically-distinct sequence stratigraphic units were defined by key element variations and correlated to previously outcrop and subsurface studies. The Woodbine Group forms an overall highstand sequence set, is dominated by argillaceous, OM-poor chemofacies deposition and contains fair quality source rock. The Eagle Ford Group is subdivided into five sequences. The Lower Member of the Lower Eagle Ford (LM-LEF) is dominated by calcareous, OM-rich chemofacies deposition and contains excellent quality source rock. The Upper Member of the Lower Eagle Ford Formation (UM-LEF) is dominated by transitional, OM-moderate chemofacies deposition and contains fair-to-good quality source rock. The Lower Member of the Upper Eagle Ford (LM-UEF) is dominated by transitional, OM-poor chemofacies deposition and contains poor quality source rock. Together the LM-LEF, UM-LEF, and LM-UEF Formations makeup a transgressive sequence set. The Middle and Upper Members of the Upper Eagle Ford Formation (MM-UEF and UM-UEF) form an overall highstand sequence set, are dominated by argillaceous-OM poor chemofacies deposition, and contain poor quality source rock.

GEOLOGIC SETTING

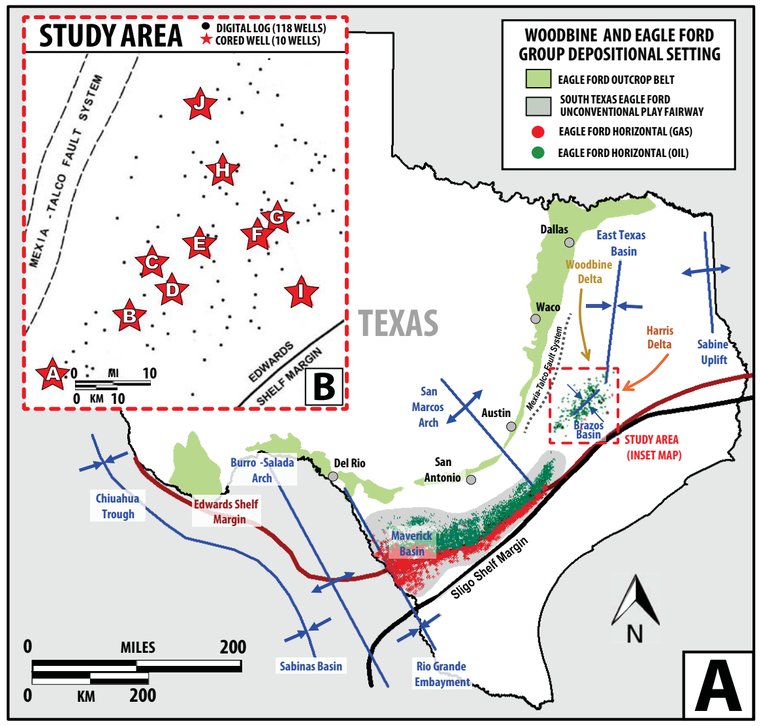

Figure 1 (Left). (A) Map of Texas showing the Eagle Ford Group outcrop belt, productive Eagle Ford Shale trend, delta systems, and major structural features during the Late Cretaceous. Modified from Wehner et al., 2017 and Donovan et al., 2015. Oil and gas well spots taken from IHS production data (IHS, 2018). **(B)** Inset map of Brazos Basin study area, core locations, and digital well log locations for this study.

Table 1. Core data (XRF, XRD, TOC) for each of the ten wells, labelled A through J, in this study.

Study Label	Core Length (ft/m)	XRF Points	XRD Points	TOC Points	Thin Sections
A	150' (46 m)	1,499	60	117	84
B	266' (81 m)	1,311	28	28	0
C	252' (77 m)	1,262	133	23	16
D	268' (81 m)	1,334	146	52	15
E	270' (82 m)	1,350	20	121	44
F	209' (64 m)	1,047	44	101	24
G	300' (91 m)	1,491	84	178	50
H	250' (76 m)	1,205	24	25	0
I	89' (27 m)	437	84	63	0
J	272' (83 m)	1,346	0	0	0
TOTAL	2,326'	12,282	623	708	233

Figure 2. (Right) Late Cretaceous chronostratigraphy showing both classic and new International Commission on Stratigraphy (ICS) stage boundaries. Macrofaunal zones, mega-cycles, and δ13C global isotope profiles are derived from the work of Ogg and Hinnov (2012). Modified with permission from Donovan et al. (2019).

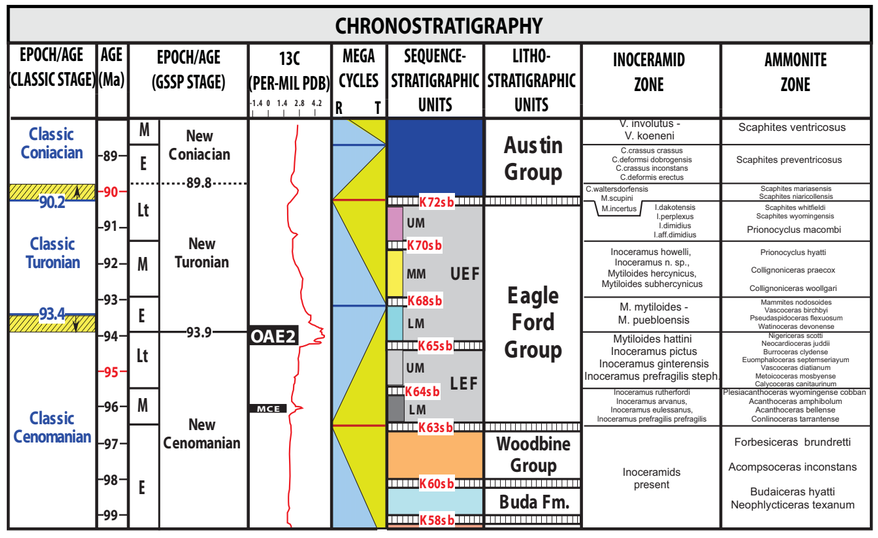

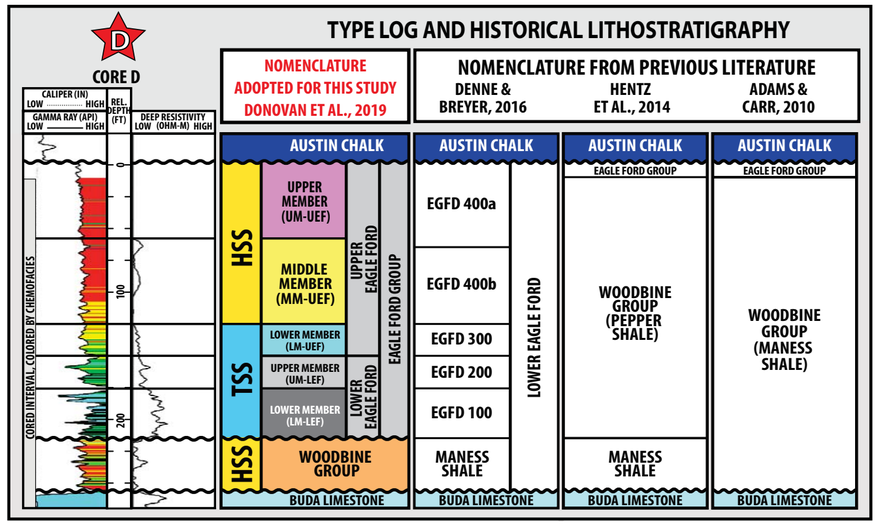

Figure 3. (Left) Type log (Core D) for the Eagle Ford and Woodbine Groups in the Brazos Basin. The stratigraphic nomenclature adopted for this study, based on work by Donovan et al. (2015, 2019), is shown directly right of the type log. Nomenclatures from previous literature are derived by correlating from published cross-sections to the Core D (Adams and Carr, 2010; Hentz et al., 2014; Denne and Breyer, 2016). The gamma-ray log is colored by core-derived chemofacies.

METHODOLOGY

HIGH-RESOLUTION XRF AQUISITION

Energy dispersive x-ray fluorescence (ED-XRF) data were collected using two Bruker Tracer 5i handheld spectrometers on all ten cores. Data were collected every 1.2" (3.0 cm) on Core A and every 2.4" (6.0 cm) on the remaining cores (Cores B through J). Significant testing (Figure 4) was conducted on Core F to establish the following collection parameters for this study.

Three elements were poorly detected by the handheld: Cu, Ba, and U; these data were therefore omitted from the study. Significantly high concentrations of Ca (>25%) interfere with the detection of many trace elements (e.g. Ni, V, Mo, Cr, Zn). Therefore, any data showing this interference was removed when portraying cross-plot relationships of these trace elements with other data. At any point where a plug was extracted for XRD mineralogy or TOC data analysis, care was taken to collect an XRF measurement as close as possible to the plug hole.

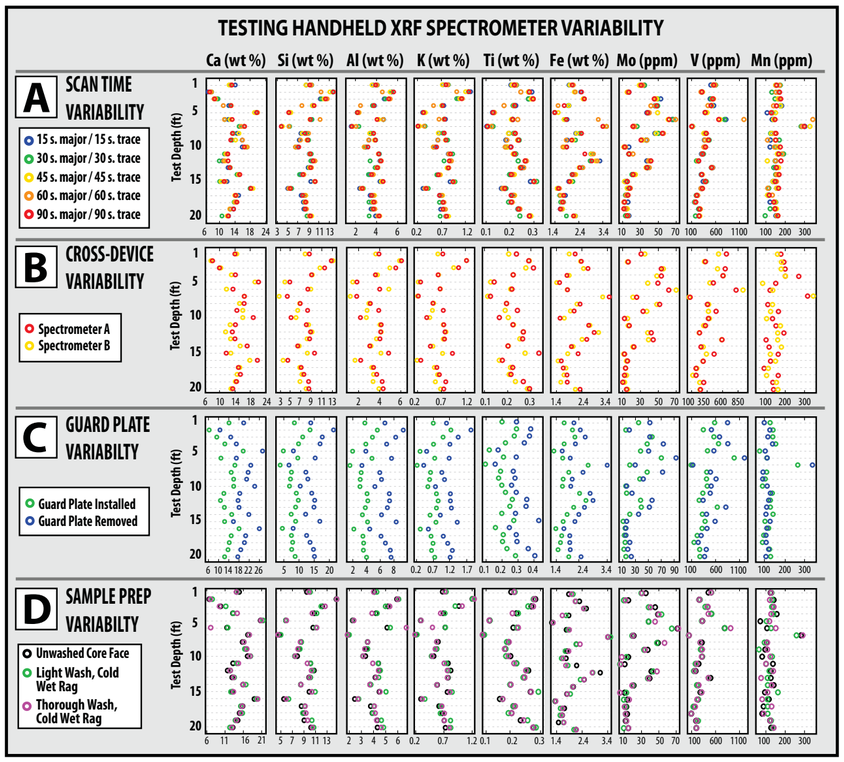

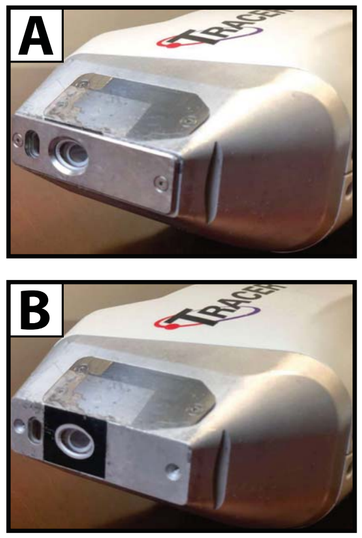

Figure 5. (Above) Photographs of handheld Bruker Tracer 5i spectrometer **(A)** with guard plate installed and **(B)** with guard plate removed. The guard plate increases the distance between the scintillometer and the core slab face, attenuating photo energy and decreasing detected concentrations. It was removed during the collection of XRF data used within this study.).

Figure 4. (Above Right) Testing conducted at selected depths to determine the most optimal procedures of use for the Bruker Tracer 5i handheld x-ray spectrometers. **(A)** Testing conducted for various scanning time intervals. **(B)** Testing conducted between the two identically-calibrated handheld spectrometers, A and B, used in this study. **(C)** Testing conducting with and without the metal guard plate that comes pre-installed on the spectrometers and can be unscrewed and removed (see Figure 5). **(D)** Testing conducted between unwashed, lightly washed, and thoroughly washed samples.

SPOTFIRE DENDOGRAM TO DELINEATE CHEMOFACIES

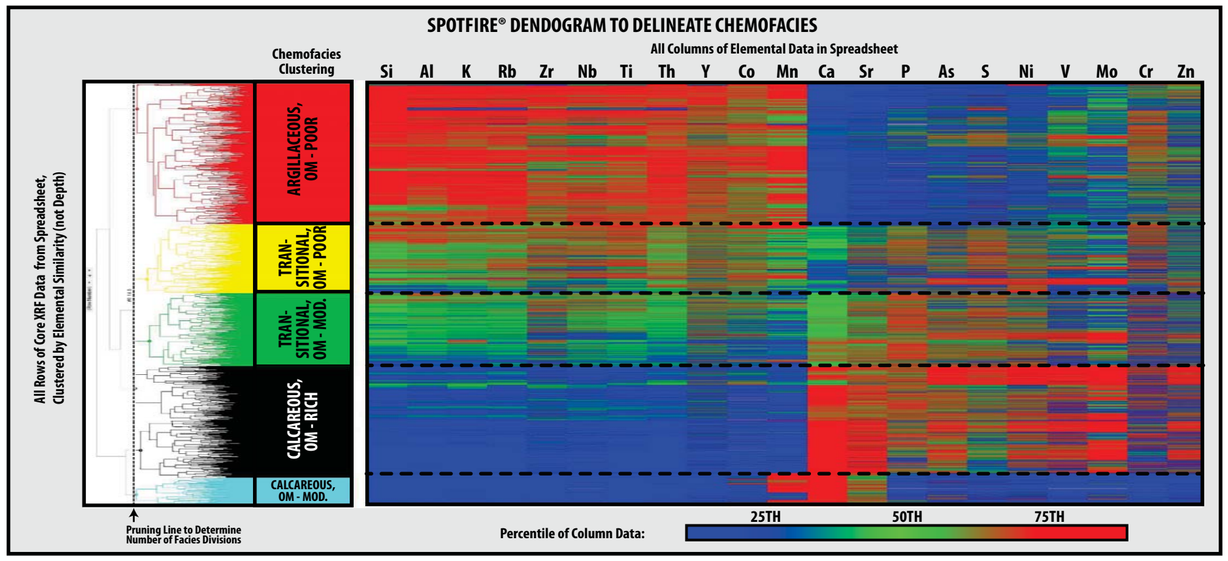

Figure 6. Dendogram visualization tree produced in TIBCO Spotfire® application used to sub-divide all elemental data across all cores into five chemofacies. Each column in the figure represents a column of elemental data in the spreadsheet of data for this study. Each row in represents a row of data in the spreadsheet tagged with one depth and one core name. The rows are not organized by depth or core; they are clustered based on the similarity of the elemental data in each column. This effectively allows the grouping of elementally-similar XRF data points across all cores.

PETROGRAPHIC DESCRIPTIONS

Table 2. Bioturbation index from Lazar et al. (2015) used to characterize sedimentological observations made in thin sections.

Bioturbation Index	Observed Features	Interpretation
0	No burrows visible; primary sedimentary structures preserved	*Not bioturbated*
1	Beds continuous, but a few burrows	*Weakly bioturbated*
2	Beds discontinuous, some burrows	*Sparsely bioturbated*
3	Remnant bedding, burrows common	*Mostly bioturbated*
4	Very little bed continuity, burrows abundant	*Strongly bioturbated*
5	No remnant bedding, fully homogenized	*Churned*

Table 3. Five classifications for common sedimentary textures observed petrographically in this study and corresponding interpretations for depositional energy.

Sediment Energy Index	Observed Features	Interpretation
0	No scour surfaces, no mud rip-up intraclasts, no ripples, no graded laminations	*Lowest energy, no evidence of storms or currents*
1	Scour surfaces, mud rip-up intraclasts	*Low energy, little evidence of currents and storms*
2	Scour surfaces, mud rip-up intraclasts, fragmented skeletal grains, ripples	*Moderate energy, moderate evidence of currents and storms*
3	Scour surfaces, mud rip-up intraclasts, fragmented skeletal grains, ripples, graded planar laminations	*High energy, moderate evidence of currents, waves, and storms*
4	Scour surfaces, mud rip-up intraclasts, fragmented skeletal grains, ripples, graded planar laminations with medium to course size quartz grains	*Highest energy, signifcant evidence of currents, waves, and storms*

STRATIGRAPHIC CHARACTERIZATION

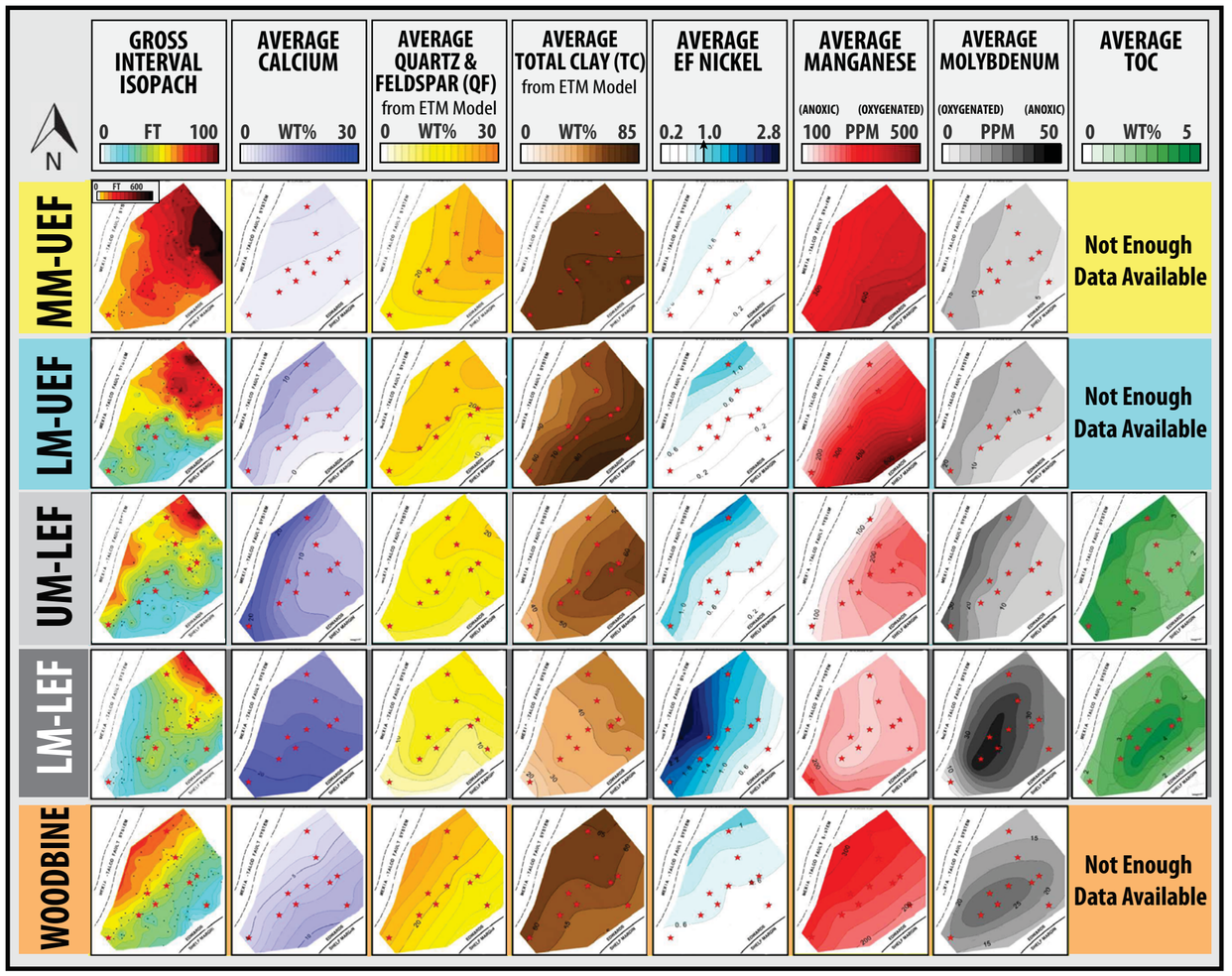

Figure 18. Gross interval isopach, average elemental, and average TOC maps for each stratigraphic unit. For each column of map sets, maps were color-scaled the same, such that relative changes across unit can be conceptualized. All elemental maps were constructed by contouring the average value per stratigrpahic unit in each cored well across the basin. Average quartz and feldspar (QF) and total clay (TC) concentrations were calculated on cored wells using the element-to-mineral conversion model.

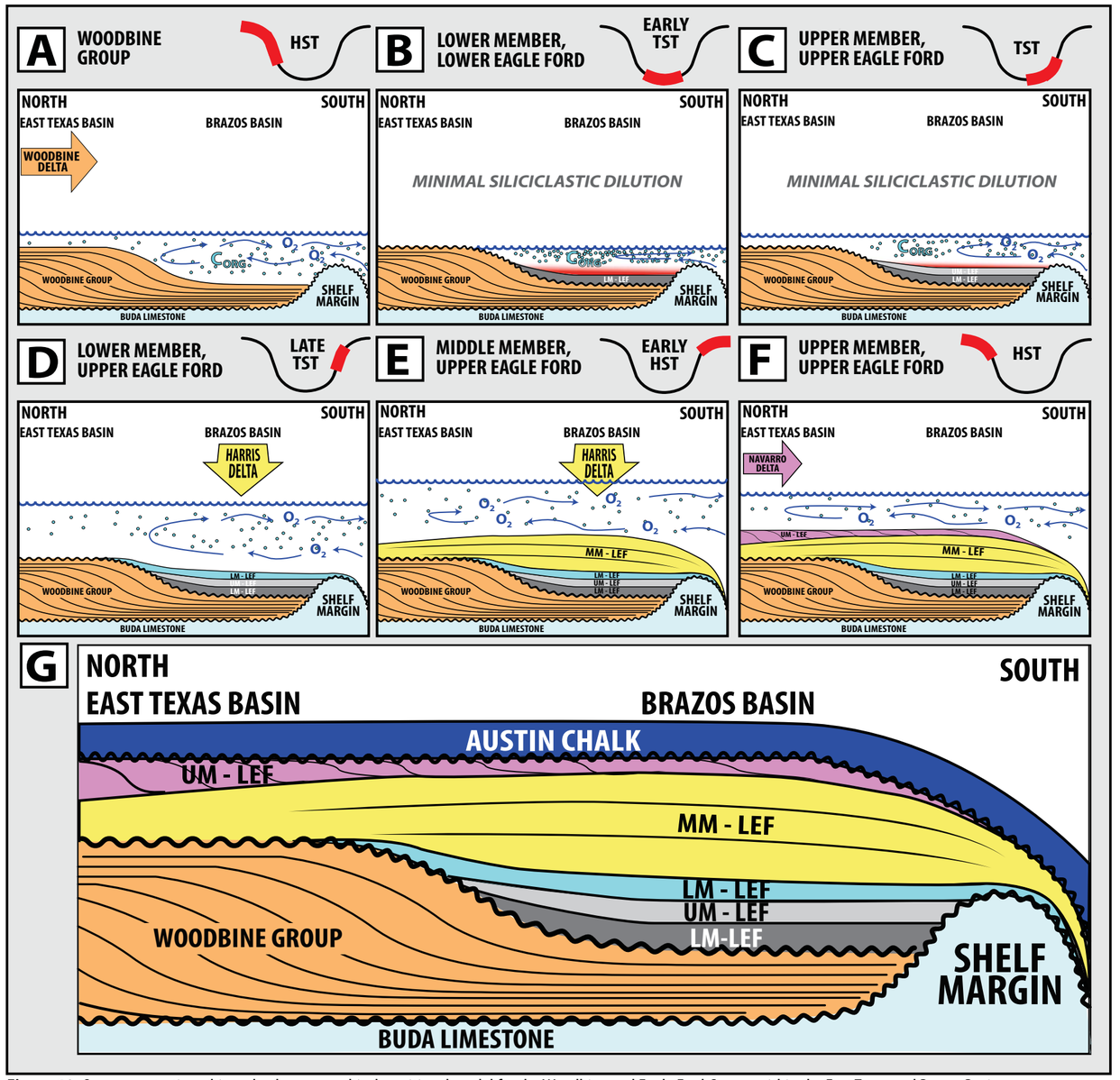

Figure 19. Sequence stratigraphic and paleogeographic depositional model for the Woodbine and Eagle Ford Groups within the East Texas and Brazos Basins.

CONCLUSIONS

Mudstone deposition is complex even in the simplest of shale formations and depends on a variety of depositional processes. Often, variability is only discernible on the micro-scale and requires a higher-resolution analysis, especially when utilizing cores. XRF data is inexpensive, simple to collect across many cores, and can be correlated to TOC and XRD mineralogy. When corroborated petrographically, elemental proxies for mineralogy and organic-matter richness provide the basis for interpretation of chemostratigraphic boundaries and changes in regional depositional processes occurring within a shale basin. In the Woodbine and Eagle Ford Groups in the Brazos Basin, several key elements are identified and correlated to depositional conditions: (1) Ca indicates carbonate input, which is dominated by OM-rich planktonic fecal pellet deposition; (2) Si + Ti + Al + K indicates OM-lean terrigenous clay; (3) Mo and Mn are inverse indicators of redox conditions during deposition—high Mo and low Mn concentrations are generally favorable for OM preservation and enrichment; and (4) Ni records paleoproductivity and is favorable for OM deposition and enrichment.

Five statistically-clustered chemofacies were identified from elemental analysis throughout the Woodbine and Eagle Ford Groups: (1) argillaceous, OM-poor; (2) transitional, OM-poor; (3) transitional, OM-moderate; (4) calcareous, OM-rich; and (5) calcareous, OM-moderate. These chemofacies highlight the high-frequency variability within an often macroscopically-homogeneous shale and have direct relationships with OM-richness. The argillaceous, OM-poor chemofacies represents the proximal facies with the most oxygenated, high-energy depositional conditions. The calcareous, OM-rich chemofacies represents the most distal facies with the least oxygenated, low-energy depositional conditions. Petrographic observations of current and bioturbation indicators suggest that the most oxygen-restricted chemofacies was deposited in, at most, intermittently anoxic depositional conditions. In fact, all chemofacies are interpreted to be deposited an intra-shelf basin above storm-wave-base.

Five chemically-distinct temporal packages are defined by variations in dominantly occurring chemofacies and major elemental shifts that coincide with major stratigraphic surfaces proposed by Donovan et al. (2018, 2019). The Woodbine Group, an overall highstand sequence set, is dominated by argillaceous, OM-poor chemofacies deposition, responding to siliciclastic input from the northwesterly-sourced Woodbine Delta. Deposition occurred in oxygenated conditions with moderate OM productivity resulting in fair-to-poor source rock quality. The erosional unconformity between the Woodbine and Eagle Ford groups is geochemically documented by the abrupt transition from argillaceous, OM-poor to calcareous, OM-rich chemofacies deposition. The LM-LEF, UM-LEF, and LM-UEF Formations comprise an overall transgressive sequence set and contain the least amounts of OM-lean terrigenous clay, which dilute the OM-rich, planktonic fecal pellet background suspension settling occurring on the shelf at this time. The LM-LEF Formation is dominated by calcareous, OM-rich chemofacies deposition on a dysoxic shelf, resulting in excellent-quality source rock. The UM-LEF Formation is dominated by calcareous, OM-moderate chemofacies deposition on an oxygenated to dysoxic shelf, resulting in fair-quality source rock. The LM-UEF Formation is dominated by transitional, OM-poor chemofacies deposition on an oxygenated shelf, resulting in poor-quality source rock. The MM-UEF and UM-UEF together comprise a highstand sequence set and are both dominated by argillaceous, OM-poor chemofacies deposition, responding to siliciclastic input from the northeasterly-sourced Harris Delta. Deposition occurred on an oxygenated shelf with low OM-productivity resulting in poor-quality source rock.

REFERENCES

Adams, R. L., and J. P. Carr, 2010, Regional depositional systems of the Woodbine, Eagle Ford, and Tuscaloosa of the U.S. Gulf Coast: The Gulf Coast Association of Geological Societies Transactions, v. 60, p. 3-27.

Adkins, W. S., and F. E. Lozo, 1951, Stratigraphy of the Woodbine and Eagle Ford, Waco area, Texas: In F. E. Lozo, ed., The Woodbine and adjacent strata of the Waco area of Central Texas, A symposium for the 1951 East Texas Geological Society Fieldtrip, p. 101–163.

Al Duhailan, M., Sonnenberg, S., and M. Longman, 2015, Analyzing "Beef" fractures: Genesis and relationship with organic-rich shale facies: Unconventional Resources Technology Conference (URTeC).

Algeo, T. J., and H. Rowe, 2012, Paleoceanographic applications of trace-metal concentration data: Chemical Geology, v. 324-325, p. 6-18.

Bohacs, K. M., G. J. Grabowski, A. R. Carrol, P. J. Mankiewicz, K. J. Miskell-Gerhardt, J. R. Schwalbach, and M. B. Wegner, 2005, Production, Destruction, and Dilution- the many Paths to Source-Rock Development: Society for Sedimentary Geology. v. 82, p. 61-101.

Brumsack, H. J., 2006, Trace metal content of recent organic carbon-rich sediments: Implications for Cretaceous black shale formation: Palaeogeophraphy, Palaeclimatology, Palaeoecology, v. 232, p. 344-361.

Brumsack, H.J., 1989, Geochemistry of recent TOC-rich sediments from the Gulf of California and the Black Sea: Geologische Rundschau, v. 78, no. 3, p. 851-882.

Denne, R. A. and J.A. Breyer, J., 2016, Regional Depositional Episodes of Cenomanian-Turonian Eagle Ford and Woodbine Groups of Texas. In R. A. Denne and J. A. Breyer, The Eagle Ford Shale: A renaissance in U.S. oil production: AAPG Memoir 110, p. 87-133.

Donovan, A. D., R.D. Gardner, A. Pramudito, T.S. Staerker, M. Wehner, M.J. Corbett, and K.S. Boling, 2015, Chronostratigraphic relationships of the Woodbine and Eagle Ford Groups across Texas: Gulf Coast Association of Geological Societies Transactions, v. 4, p. 67-87.

Donovan, A. D., T. S. Staerker, A. Pramudito, W. Li, M. J. Corbett, C. M. Lowery, A. M. Romero, and R. D. Gardner, 2012, The Eagle Ford outcrops of west Texas: A field laboratory for understanding heterogeneities within unconventional mudstone reservoirs: GCAGS Journal, v. 1, p. 162–185

Donovan, A. D., T.S. Staerker, R. Gardner, M.C. Pope, M. C., A. Pramudito, and M. Wehner, 2016, Findings from the Eagle Ford Outcrops of West Texas and Implications to the Subsurface of South Texas: In R. A. Denne and J. A. Breyer, The Eagle Ford Shale: A renaissance in U.S. oil production: AAPG Memoir 110, p. 301-336.

Donovan, A.D., M.J. Meyer, A. Pramudito, and M.C. Pope, Unraveling the Secrets of the "Eaglebine": Using Sequence- and Chemo-Stratigraphy to Differentiate Unconventional Plays and Play Fairways within the Woodbine and Eagle Ford Groups in the East Texas Basin: The Houston Geological Society Bulletin, v. 61, no. 3, p. 22.

Donovan, A.D., S. Gifford, A. Pramudito, M.J. Meyer, and M.C. Pope, Unraveling the Secrets of the "Eaglebine": Unconventional Resources Technology Conference (URTeC).

Hentz, T. F. and S.C. Ruppel, 2010, Regional lithostratigraphy of the Eagle Ford Shale: Maverick Basin to East Texas Basin: Gulf Coast Association of Geological Societies Transactions, v. 60, p. 325-337.

Hentz, T. F., W. A. Ambrose, and D. C. Smith, 2014, Eaglebine play of southwestern East Texas basin: Stratigraphic and depositional framework of the Upper Cretaceous (Cenomanian-Turonian) Woodbine and Eagle Ford Groups: AAPG Bulletin, v. 98, no. 12, p. 2551-2580.

Hudson, A. M., 2014, Stratigraphy and Depositional Controls on Source Rock Formation within the Upper Cretaceous (Lower Cenomanian) Maness Shale, Central Texas, Master's Thesis, Texas A&M University, College Station, Texas.

IHS Energy Group, 2018, U.S. well and production data: Englewood, Co, IHS Energy Group.

Katz, B. J., 2012, Controlling Factors on Source Rock Development- A Review of Productivity, Preservation, and Sedimentation Rate: Society for Sedimentary Geology Special Publications, v. 82, p. 7-16.

Lazar, O. R., K.M. Bohacs, J.H. Macquaker, J. Schieber, and T.M. Demko, 2015, Capturing key attributes of fine-grained sedimentary rocks in outcrops, cores, and thin sections: nomenclature and description guidelines: Journal of Sedimentary Research, v. 85 no. 3, p. 230-246.

Mancini, E. A., and T. M. Puckett, 2005, Jurassic and Cretaceous transgressive-regressive (TR) cycles, northern Gulf of Mexico, USA: Stratigraphy, v. 2 no. 1, p. 31-48.

Mancini, E. A., P. Li, D. A. Goddard, V. Ramirez, and S. C. Talukdar, 2008, Mesozoic (Upper Jurassic-Lower Cretaceous) deep gas reservoir play, central and eastern gulf coastal plain: AAPG Bulletin, v. 92, p. 283-308.

Minisini, D., J. Eldrett, S.C. Bergman, and R. Forkner, 2018, Chronostratigraphic framework and depositional environments in the organic-rich, mudstone-dominated Eagle Ford Group, Texas, USA: Sedimentology, v. 65, no. 5, p. 1520-1557.

Ogg, J. G., and L. A. Hinnov, 2012, Cretaceous: In F. M. Gradstein, J. G. Ogg, M. Schmitz, and G. Ogg, eds., The geologic time scale: Elsevier (Amsterdam), p. 793–853.

Oliver, W. B., 1971, Depositional Systems in the Woodbine Formation (Upper Cretaceous), Northeast Texas: The University of Texas at Austin: Bureau of Economic Geology Report of Investigations, v. 73.

Sageman, B. B., and T.W., Lyons, 2004, Geochemistry of fine-grained sediments and sedimentary rocks: Sediments, Diagenesis, and Sedimentary Rocks, v. 7, p115-158.

Schieber, J, 2003, Simple gifts and buried treasures—implications of finding bioturbation and erosion surfaces in black shales: The Sedimentary Record, v. 1, no. 2, p. 4-8.

Schieber, J., R. Lazar, K. Bohacs, R. Klimentidis, M. Dumitrescu, and J. Ottmann, 2016, An SEM study of porosity in the Eagle Ford Shale of Texas—Pore types and porosity distribution in a depositional and sequence-stratigraphic context, p. 167-186.

Taylor, S. R., and S. McClennan, 1985, The Continental Crust: its Composition and Evolution. Oxford: Blackwell Scientific Publications, p. 312.

Tribovillard, N., Algeo, T. J., Baudin, F., & Riboulleau, A. (2012). Analysis of marine environmental conditions based onmolybdenum–uranium covariation—Applications to Mesozoic paleoceanography. Chemical Geology, 324, 46-58.

Tribovillard, N., T.J. Algeo, T. Lyons, and A. Riboulleau, 2006, Trace Metals as Paleoredox and Paleoproductivity Proxies: An Update: Chemical Geology, v. 232, p. 12-32.

Wedepohl, K.H., 1970, Environmental influences on the chemical composition of shales and clays: Physics and Chemistry of the Earth, v. 8, p. 305-333.

Wehner, M., R.D. Gardner, M.C. Pope, and A.D. Donovan, 2017, The Eagle Ford Group Returns to Big Bend National Park, Brewster County, Texas: Gulf Coast Association of Geological Societies Transactions, v. 6, p. 161-176.

Wilson, R. D., J. Schieber, 2017, Association Between Wave-and Current-aided Hyperpycnites and Flooding Surfaces in Shelfal Mudstones: an Integrated Sedimentologic, Sequence Stratigraphic, and Geochemical Approach: Journal of Sedimentary Research v. 87 no. 11, p. 1143-1155.

AUTHOR VITAE

Melissa J. Meyer
Apache Corporation
Houston, TX

Melly Meyer received her M.S. degree in Geology in 2018 from Texas A&M University. Employed as a geologist with Apache Corporation since 2015, she has primarily worked on projects in the Gulf Coast and in Permian Basin. Her current research interests include the application of sequence stratigraphic, chemostratigraphic, and petrographic techniques in mudstones to assess unconventional resource potential in shale basins.

Arthur D. Donovan
Department of Geology and Geophysics - Texas A&M University
College Station, TX

Art Donovan received his Ph.D. from the Colorado School of Mines in 1985. After a 30-year career holding both technical and management roles at Exxon and BP, he joined Texas A&M University as full-time faculty in 2016. At TAMU, Art is the director of the UROC Consortium, whose research focuses on outcrop and sub-surface studies of conventional and unconventional reservoirs.

Michael C. Pope
Department of Geology and Geophysics - Texas A&M University
College Station, TX

Mike Pope earned an Earth and Space Science degree (B.S. 1985) from UCLA, and Geology degrees from the University of Montana (M.S. 1989) and Virginia Tech (Ph.D, 1995). He worked for Mobil Oil and taught at Washington State University before moving to Texas A&M University in 2009. He teaches courses in carbonate depositional systems, sequence stratigraphy, and field camp.

ACKNOWLEDGEMENTS

This research was supported primarily through funding, core access, and rock data from Apache Corporation. Hawkwood Energy also provided several cores, rock data, and permission to publish. This work would not have been possible without the mentorship of Ann Hudson, Tad Smith, Brian Coffey, Casey Donohue, Travis Johnston, Martin Gibson, and Mark Olson. Frank Sheppard's managerial approval to conduct and publish this study is greatly appreciated. We thank Michael Ashby for permission to use his element-to-mineral conversion program.